EUROPEAN ORGANIZATION FOR NUCLEAR RESEARCH

CERN–PPE/95–73
18 May 1995

Charged particle multiplicity and transverse energy measured in ^{32}S central interactions at 200 GeV per nucleon

S. AOKI[7,a] V. BISI[11], A. C. BRESLIN[4], F. CASSOL[2], M. G. CATANESI[2], D. H. DAVIS[6], A. DI BARTOLOMEO[9], S. DI LIBERTO[8], M. J. ESTEN[6], P. GIUBELLINO[11], G. GRELLA[9], K. HOSHINO[7], M. KAZUNO[10], M. KOBAYASHI[7], K. KODAMA[1], S. LUSSO[11], A. MARZARI-CHIESA[11], M. MASERA[11], F. MEDDI[8], M. MIYANISHI[7], M. T. MUCIACCIA[2], S. NAKANISHI[7,b] K. NAKAZAWA[5], K. NIU[7], K. NIWA[7], M. NOMURA[7], G. POULARD[3], L. RAMELLO[11], L. RICCATI[11], G. ROMANO[9], G. ROSA[9], M. S. SARTORI[11], C. SGARBI[8], H. SHIBUYA[10], S. SIMONE[2], H. TAJIMA[7,b] D. N. TOVEE[6], N. USHIDA[1], T. VIRGILI[8,c].

1. Aichi University of Education, Kariya, Japan.
2. Dipartimento di Fisica dell' Università and INFN, Bari, Italy.
3. CERN, Geneva, Switzerland.
4. Department of Physics, University College Dublin, Dublin, Ireland.
5. Faculty of Education, Gifu University, Gifu, Japan
6. Department of Physics & Astronomy, University College London, London, UK.
7. Department of Physics, Nagoya University, Nagoya, Japan.
8. Dipartimento di Fisica, Università 'La Sapienza' and INFN, Rome, Italy.
9. Dipartimento di Fisica Teorica e SMSA dell'Università and INFN, Salerno, Italy.
10. Department of Physics, Toho University, Funabashi, Japan.
11. Dipartimento di Fisica Sperimentale dell' Università and INFN, Turin, Italy.

Submitted to IL NUOVO CIMENTO A

[a]Now at Kobe University, Kobe, Japan.
[b]Now at University of California,Santa Barbara, USA.
[c]Now at University of Salerno and INFN,Salerno, Italy.

Abstract. - Interactions induced by 200 GeV per nucleon ^{32}S ions on heavy targets were selected by the HELIOS calorimeters and studied in nuclear emulsions. Global observables, such as charged particle multiplicity and transverse energy, were determined event-by-event. Multiplicity and transverse energy were measured as a function of the pseudorapidity over the large acceptance of the present experiment ($0.6 \leq \eta \leq 5.5$). A comparison of the experimental data with those provided by the event generators FRITIOF and VENUS shows remarkable differences both in the target spectator region and in the participant region. An attempt is made to interpret these discrepancies in terms of plausible mechanisms, like baryon-pair production or rescattering.

PACS 25.75 - Relativistic heavy-ion nuclear reactions.

1 - Introduction.

In the search for a transition from ordinary hadron matter to a deconfined chiral-symmetric quark-gluon plasma (QGP), ultra-relativistic heavy-ion collisions have been extensively studied in the last few years[1]. The initial experimental activity, successfully dealing with huge hadronic showers, demonstrated that a high enough energy density, a prerequisite for deconfinement, is attainable in central collisions. However signatures of a phase transition, previously anticipated as unambiguous, such as J/ψ suppression or strangeness enhancement, indeed observed, were put in question, revised and somehow incorporated in less exotic schemes[2]. On the other hand, both QCD lattice calculations defining the plasma phase and first attempts to put forward a quark-gluon transport theory progressed slowly[3-5].

Whereas experiments with beams of much heavier ions, now collecting data both at CERN and at BNL, will probably clarify at least some of the many open questions, it is worth comparing the available data with calculations based on conventional physics. In fact, at present, any mismatch between data and predictions could hardly be claimed as an unambiguous signal of a phase transition, but just shows that complex beam-target interactions cannot be treated as a superposition of independent nucleon-nucleon collisions. At least, more realistic models of conventional physics should be attempted, taking benefit from the amount and quality of the available data.

In this paper we present the analysis of a sample of interactions induced by 200 GeV per nucleon ^{32}S ions, selected by transverse energy, $E_{\rm T}$, and studied in nuclear emulsions. The accurate measurement on each event of both charged particle multiplicity and transverse energy is a unique feature of the present experiment. This work considerably improves our previous results[6], in particular due to the increased statistics and to the wider pseudorapidity range, now spanning from the target fragmentation region up to the projectile fragmentation region.

2 - Experimental procedure.

Nuclear emulsion stacks were exposed to a 200 GeV per nucleon ^{32}S beam in the target region of the HELIOS (High-Energy Lepton and IOn Spectrometer) apparatus at CERN[7,8]. A Si micro-strip beam hodoscope was used to locate the interactions in the stack; a charge-multiplicity Si counter in the form of adjacent segmented rings (in total 384 pads) was used in the selection. The emulsion pellicles were set perpendicular to the beam. Some of the stacks included W target sheets interleaved with the emulsion pellicles so that both interactions in the composite emulsion medium and in the heavy target could be studied.

The wide-angle region ($\eta \leq 3$) was covered by U-Cu/scintillator and Fe/scintillator tower-structured sampling calorimeters, the forward region ($\eta \geq 3$) was covered by a highly segmented U/liquid argon calorimeter (ULAC). Due to the position of the emulsion target, 42.6 cm up-

stream of the standard HELIOS target, the pseudorapidity coverage was $0.1 \leq \eta \leq 5.5$ instead of $-0.1 \leq \eta \leq 5.5$; the target shift also implied a small overlap of backward and forward calorimeters, and the effect was taken into account in the off-line analysis by correcting the value of the measured E_{T} accordingly.

In order to enrich the data with central interactions, while keeping a sample of (nearly) unbiased events, the physics trigger was set with different E_{T} thresholds on the wide angle calorimeters, and the fraction of recorded events with low E_{T} was reduced by pre-set down-scaling factors. Interactions to be studied in emulsion were selected off-line mostly at high E_{T}, but a number of them was also sampled at lower E_{T} for reference. We note here that, although nuclear emulsion is a composite target, a sufficiently high E_{T}-cut selects interactions on the heaviest elements (Ag and Br). Indeed, in such a case, even the contribution from Br is marginal, hence we will refer to an Ag target in connection with high E_{T} S-emulsion data.

The selected interactions were located and the tracks of all the outgoing charged particles measured in emulsion to determine their angles with respect to the beam direction. The measurements were performed close to the primary vertex, within $\approx$ 1 mm, and thus the multiplicity does not include contributions from secondary activity and non-prompt decays. This procedure just allowed the inclusion of a few electron pairs whose vertices were not detectable. It is estimated that they contribute to not more than 2 % of the charged multiplicity.

More details about the experimental set-up, data-taking and measurement procedure can be found in references[6-9].

The charged particle multiplicity considered in the following refers solely to close-to-minimum ionizing particles ("shower tracks"), while heavily ionizing particles ("black" and "grey" prongs) were excluded. For resolution and efficiency reasons we restricted ourselves to charged particle multiplicity and transverse energy in the pseudorapidity range $(0.6 \leq \eta \leq 5.5)$.

The final data sample consists of 215 S-Ag and 175 S-W interactions.

3 - Models of nucleus-nucleus collisions.

3.1 - Event generators.

We compared our data with two widely used event generators, VENUS[10] and FRITIOF[11]. Both generators belong to the class of string models, the main difference between them being the basic mechanism for string formation (colour exchange for VENUS, momentum exchange for FRITIOF). In the case of VENUS we used two versions, namely 3.11 and 4.12, because the first was extensively used in the past for a comparison with experimental data, but the second is much more reliable according to the authors, and contains numerous improvements. Further attempts are in progress to implement VENUS[12] and other string-model inspired codes, like DPM and QGSM[13], in order to cope with both higher string densities, already relevant in

nucleus-nucleus collisions at SPS energies, and hard scattering processes, of growing importance at RHIC and LHC energies. In these models, as in several others, nucleus-nucleus collisions are treated as a linear superposition of nucleon-nucleon interactions. The number of primary collisions, and thus the number of participating constituents, is determined by the geometry of the collision, i. e. by the impact parameter b. The transverse energy flow is then proportional to the number of participant nucleons.

Still in the framework of conventional physics, the Relativistic Quantum Molecular Dynamical model, RQMD[14] - an extension of concepts previously applied to intermediate-energy nucleus-nucleus collisions - was recently proposed. It postulates the formation of "colour ropes" within a high string density. The coded RQMD was successfully compared with AGS data[15], and the comparison is being extended to SPS data[16].

An alternative approach could be provided by hydrodynamical models[17]. Here, nuclear matter is treated as an expanding relativistic fluid, allowing the formation of QGP under appropriate initial conditions. Numerical calculations based on these models, that still contain several untested assumptions, were recently performed and compared with several sets of nucleus-nucleus data [5,18]. Since the purpose of this paper is to present our experimental results and to compare them with relatively simple and well established models, at present we will confine our attention to FRITIOF and VENUS.

Minimum-bias ^{32}S-Ag and ^{32}S-W interactions were generated by VENUS 3.11 and 4.12, and FRITIOF 1.6, with no change in their standard parameters. However, in order to compare directly these data with emulsion measurements, charged particles generated with low momenta were not considered and the decay of strange particles, both mesons and baryons, was inhibited. In fact, low momentum charged particles, mostly emitted at large angles, appear in emulsion as "grey" prongs (see section 2), whereas strange particles have long decay paths and their decay products are not seen close to the primary vertex. Indeed, removal of low momentum particles turned out to have a negligible effect in our angular acceptance, but the inhibition of strange particle decays affects considerably the charged particle multiplicity of the generated events, which decreases by 7% to 10%. Of course, this procedure slightly affects the E_{T} distributions, but the effect turned out to be marginal due to the granularity of the calorimeters.

Figure 1 shows the E_{T} distributions of the generated events on Ag and W, and the differential cross-section $\frac{d\sigma}{dE_{\mathrm{T}}}$ reported by HELIOS[8] on the same targets. The normalisation of simulated to experimental values has been performed according to the procedure shown in section 3.2. Both versions of VENUS gave almost identical results, indistinguishable on the scale of figure 1. All the distributions are similar, with a wide plateau followed by a steeply falling tail. Indeed, $\frac{d\sigma}{dE_{\mathrm{T}}}$ essentially reflects the geometry of the collision, and the shoulder of the curve corresponds to full overlap of the colliding nuclei. Thus the E_{T} variable is a valuable tag for impact parameter.

It is seen, however, that FRITIOF fails to reproduce the high-E_{T} tail of the measured differential cross-sections, while the agreement with VENUS, both versions, is considerably

better. This better agreement must be ascribed to intra-nucleus rescattering, taken into account in VENUS[10].

3.2 - Normalization procedure and event classification.

In order to compare experimental data with models in terms of centrality, a suitable normalization procedure was adopted because a mismatch in $\frac{d\sigma}{dE_T}$ prevents a straightforward selection based on events within given intervals of E_T. Indeed, it is very difficult to achieve an absolute normalization in nucleus-nucleus data, because unaccountably large contributions to $\sigma^{\rm inel}$ often arise from interactions with low E_T, where neither data are available nor generators are reliable.

The model-generated E_T-distributions were normalized, for each target, to the HELIOS absolute cross-sections[8] by integrating them above a given value of transverse energy E_T^0 to give the same σ^0. Then, both HELIOS and generated distributions were integrated above different values of $E_T \geq E_T^0$, and the corresponding fractions of σ^0 were determined. This procedure enabled a correspondence to be established among the E_T scales. Relative to HELIOS data, the model E_T scales were multiplied by a factor 1.00, 1.01 and 1.08 for VENUS 3.11, VENUS 4.12 and FRITIOF 1.6, respectively. Finally, an absolute scale of residual cross-sections (i.e., cross-sections integrated above a certain value of E_T) as a function of E_T was established by computing the inelastic cross-sections for collisions between hard spheres. The value of E_T^0 was arbitrarily chosen to be 150 GeV, but stable results were obtained with $(50 < E_T^0 < 200)$ GeV. In this way, two event classes, "semicentral" (SCE) and "central" (CE) respectively, were finally defined for each target, corresponding to a residual cross-section of 2% (CE) and from 8% to 2% (SCE) of the inelastic cross-section. Central interactions correspond to events where there is full overlap of projectile and target nuclei.

In order to remove trigger and selection biases, essentially for the SCE samples, a weight was assigned to each event; the weight (≥ 1) is proportional to the ratio between the known[8] value of $\frac{d\sigma}{dE_T}$ and the number of measured events at a given E_T.

A suitable number of interactions was generated by VENUS and FRITIOF with a cut on the impact parameter roughly corresponding to a residual σ^{inel} of 10%. The final samples were then selected according to the above mentioned procedure.

Table 1 shows global features of both experimental and simulated data in the different classes. Here, peripheral events have been removed from the samples. Averages over experimental values make use of the weights. Most of these data will be discussed in the next sections.

4 - Experimental results and comparison with models.

4.1 - Global observables.

Transverse energy E_{T} and charged multiplicity N_{ch} were measured independently on each selected interaction, so that a correlation between these two physical quantities could be easily established and compared with that derived from simulated events. Figure 2 shows the correlation between E_{T} and N_{ch}, both measured in the interval ($0.6 \leq \eta \leq 5.5$), and that from the events generated by means of FRITIOF and VENUS.

It is found that both experimental and generated data show a sharp correlation between E_{T} and N_{ch}, and that there is independence from the target, apart the maximum attainable values. However, whereas FRITIOF and VENUS 3.11 only slightly overestimate N_{ch} for a given E_{T}, VENUS 4.12 underestimates N_{ch}, and the discrepancy increases for high E_{T}. This is reflected in the average value of E_{T} per charged particle, as shown in Table 1. As noted by the authors of VENUS as well[10], in the new version (4.12) rescattering improves the E_{T} distributions but has little influence on N_{ch}. Finally, we note that the spread of N_{ch} for a given E_{T} is considerably larger in the experimental data than in the simulated events over the whole range of E_{T}.

If we had to interpret figure 2 as an entropy-temperature diagram[19], the continuous and monotonic trend of the data would not suggest any sign of a phase transition.

4.2 - Pseudorapidity dependence of N_{ch} and E_{T}.

More detailed information about target and projectile fragmentation and about newly produced hadrons can be obtained from differential distributions as a function of the pseudorapidity η; the wide range of η attained in this experiment allows an independent analysis of target, intermediate and projectile fragmentation regions.

Figure 3 shows the charged multiplicity distributions for the different targets and event classes, and the corresponding predictions from FRITIOF and VENUS. Table 2 represents maximum densities, mean and r.m.s. values of η obtained from a Gaussian fit to the same data. No further normalization was applied to the simulated events in order not to mask overall discrepancies.

As a general trend, it is seen that the experimental mean values of η are systematically smaller than those computed by the generators, with a discrepancy increasing for the heavier target and for central events. However, except for S-W central interactions, FRITIOF seems to reproduce well both the maximum density and the shape of the distributions whereas VENUS 3.11 shows a net excess of charged particles in the projectile region and VENUS 4.12 a lack of them, mostly in the target region.

Central interactions, in particular S-W interactions, show more asymmetric multiplicity

distributions, with a maximum density towards values of η lower than $< \eta >$. This effect is much less evident in the data produced by all the generators.

Figure 4 and table 3 show the transverse energy distributions and the results of Gaussian fits on the same samples of events, and in a way similar to that used for $N_{\rm ch}$. Here, again, the experimental values of $< \eta >$ are smaller than those obtained by the generators, and the discrepancy now increases even more for the heavier target and for central events.

In addition, the experimental distributions are systematically broader than the simulated ones. Asymmetric experimental distributions are again observed, but the effect is now more evident in the semicentral interactions on both targets. There is an overall agreement between experimental and simulated data in the projectile region, while a large discrepancy, increasing with centrality, is observed in the target region, the worse result being now provided by FRITIOF.

4.3 - Pseudorapidity dependence of $E_{\rm T}/N_{\rm ch}$.

Figure 5 shows, for the different samples, the transverse energy per charged particle, $E_{\rm T}/N_{\rm ch}$, as a function of η.

The experimental data show high values of this ratio (up to 1.0 GeV/charged particle) in the backward region, a steep decrease towards the central region, a bump around $\eta = 4$, where a value of 0.70-0.75 GeV/charged particle is attained, and again a steep decrease in the forward region. Both the shape of the distributions and the absolute value of the ratios do not depend much on the target and on the centrality of the collisions.

Results from each generator, as well, do not show an appreciable difference from sample to sample, but they differ considerably among themselves and with respect to the experimental data. In particular, FRITIOF and VENUS 4.12 show a similar trend in the backward and central regions, but VENUS 4.12 falls more steeply in the forward region; VENUS 3.11, on the contrary, shows a monotonic decrease over the whole range. Of course, most of the discrepancies can be directly inferred from the distributions shown in figures 3 and 4. For instance, the high average value of $E_{\rm T}/N_{\rm ch}$ found in VENUS 4.12 can be ascribed to some overestimate of $E_{\rm T}$ in the central region, but mainly to an underestimate of $N_{\rm ch}$ over the whole η range.

About the bump around η=4, that corresponds to a polar emission angle around θ=40 mrad, we note that this cannot arise from an instrumental effect. In fact this effect could arise either from an overestimate of $E_{\rm T}$ or an underdetermination of $N_{\rm ch}$ around η=4, but from figures 3 and 4 we don't observe any irregularity in the distributions of the experimental data that could suggest such a bias. On the other hand, the effect is found in the samples with both Ag and W targets, whereas the configuration of the corresponding emulsion stacks, and in particular the thickness of the sheets, was very different in the two cases[6]. Furthermore, an angle of 40 mrad converts into a transverse linear dimension of about 20 μm at a distance of 0.5 mm from

the vertex, zone well inside the field of view of the microscopes under the chosen magnification and hence not likely to be biased. Finally, the same angular window is completely inside the acceptance of the forward calorimeter (ULAC) of the HELIOS set-up (the junction with other calorimeters is at η=2.9), and again it is very difficult to envisage, in such conditions, any relevant source of bias.

5 - Discussion.

5.1 - Correlation between $N_{\rm ch}$ and $E_{\rm T}$.

We have shown that charged particle multiplicity and transverse energy integrated over a wide range of pseudorapidity are strongly correlated, and this allows either of them to be chosen as a tag for centrality. No other experimental data are available, at least in this range of pseudorapidity, so that no direct comparison of this correlation can be made. Though FRITIOF and VENUS 3.11 reproduce the observed correlation with just some excess of $N_{\rm ch}$ for a given $E_{\rm T}$ (figure 2), $\frac{d\sigma}{dE_{\rm T}}$ falls in FRITIOF as a consequence of too small values of $E_{\rm T}$, while it is well reproduced in VENUS (figure 1). Thus, having defined as "central" those collisions where a complete overlap of projectile and target is reached (section 3.2), FRITIOF shows an average multiplicty close to the measured one, while it is higher in VENUS 3.11. In the case of VENUS 4.12, on the contrary, a definite underestimate of $N_{\rm ch}$ is obtained (table 1).

Finally, we note that, besides their different meaning, $N_{\rm ch}$ and $E_{\rm T}$ involve the same kind of particles in different ways. For example, $N_{\rm ch}$ is dominated by charged pions that, depending on the generator, target and centrality, contribute in our samples from 73% to 81% of the total number of charged particles, whereas their contribution to $E_{\rm T}$ ranges from 36% to 45% (from 58% to 74% if the γs from π^o mesons are added as well).

5.2 - Pseudorapidity distributions.

More details can be observed from an analysis of $\frac{dN_{\rm ch}}{d\eta}$ and of $\frac{dE_{\rm T}}{d\eta}$ as functions of pseudorapidity. We note that our results in most cases are in fair agreement with those from other experiments at the same energy and with the same or similar targets, in particular EMU01[20] for multiplicity distributions on emulsion and gold targets, when the different selection in centrality is accounted for, and WA80[21] for multiplicity and $E_{\rm T}$ distributions, the latter ones within a much narrower window of η.

According to the definition of pseudorapidity ($\eta = -\ln\tan\theta/2$), this coincides with the rapidity ($y = \frac{1}{2}\ln\frac{E+p_z}{E-p_z}$) for light particles ($p >> m$), hence to a good approximation for pions. For heavier particles the approximation is worse : for example, in our conditions, it is found for baryons $< \eta > \simeq < y > +1$ at η=4. As a consequence, particles with different masses created

in the same rapidity window will show up separated if analysed in a pseudorapidity spectrum. According to this mechanism – though in our experiment we have no mass identification – it is not hazardous to interpret the forward excess of both $N_{\rm ch}$ and $E_{\rm T}$ produced by VENUS 3.11 with respect to the experimental data (figures 3 and 4) as a too copious production of baryon-antibaryon pairs, an excess not evident in the same distributions from the other generators (FRITIOF and VENUS 4.12). As an example, we show in figure 6 $dN/d\eta$ as a function of η separately for $\pi^{\pm}$, $\rm K^{\pm}$, protons and antiprotons, as it is predicted by the various generators in central S-W interactions. Obviously, in the p distribution, besides those produced in baryon-antibaryon pairs, the protons originating from target and projectile are also present in the corresponding zone of pseudorapidity. In a similar way, distributions of $dE_{\rm T}/d\eta$ are shown in figure 7, where the contribution of neutral particles has been added as well because their $E_{\rm T}$ is measured in the calorimeters, and in particular, instead of p or $\bar{\rm p}$, all the baryons (including neutrons and strange ones) were considered.

As anticipated, almost the whole excess of $N_{\rm ch}$ produced by VENUS 3.11 in the forward direction can be ascribed to the huge contribution of $\rm p\bar{p}$ pairs. On the other hand, VENUS 4.12 produces more strange particles than the other generators (also neutral ones, not shown in figure 6), in better agreement with published experimental results[1,22].

Finally, the overall deficiency of charged particles produced by VENUS 4.12 in the target region must be ascribed to the pions. In fact, charged kaons already represent about 10% of the average charged multiplicity, and even an unreasonable increase of them by a factor of 2 would not fill the gap. On the other hand, the predicted number of protons is already as much as expected (see later) and their density around $\eta = 2$ was measured directly[23] and found to be in agreement with this prediction ($\frac{dN}{dy} \approx 20$).

Surprisingly, all the generators show for pions almost the same $E_{\rm T}$ distribution as a function of η, while that for kaons nearly reproduces the corresponding charged multiplicity distribution. On the contrary, there is a large excess of $E_{\rm T}$ in the forward region in VENUS 3.11 with respect to other generators in the sample of antibaryons, but less apparent than that of $N_{\rm ch}$ in the same zone because the number of produced $\bar{\rm n}$ is only $\simeq$40% that of $\bar{\rm p}$. In the $E_{\rm T}$ distribution of baryons, finally, there is a very large density in the backward region in VENUS 4.12, a factor of 2 to 4 larger than in FRITIOF, and this is due not only to the larger contribution from Λs, but also to the unexpectedly large value of $E_{\rm T}$ per baryon (from 0.5 to 1.1 GeV at η=2, as compared to 0.25 to 0.7 GeV from FRITIOF).

In order to have a more quantitative comparison among the generators, we show in Table 4 the predicted net number of baryons (number of baryons minus number of antibaryons), subdivided into charged and neutral, and the total number of antibaryons (of any charge) within the interval $0.6 \leq \eta \leq 5.5$. Data from the generators refer to the classes of the events considered up to now. As a comparison, we also show the number of nucleons (N Max) expected to be involved in an interaction with impact parameter $b = 0$. We note that both versions of VENUS give similar figures for the net number of baryons, but VENUS 3.11 does not reproduce the

isotopic composition of the system projectile-target. Moreover, VENUS involves systematically more baryons than FRITIOF, and in some case, like in central S-W interactions, more than those foreseen by complete overlap (and even more, if those outside the angular acceptance are taken into account). This is certainly due to the fact that rescattering was included in these versions of VENUS, so that some of the spectator nucleons are involved as well.

5.3 - Transverse energy per charged particle.

The discussion of the data shown in figure 5 is more complicated, because any discrepancy between experimental data and simulations in the ratio $E_{\rm T}/N_{\rm ch}$ for a given value of η could depend on many quantities, in particular the real fraction of neutral and charged particles, and the same effect could be ascribed either to a discrepancy in $E_{\rm T}$ or in $N_{\rm ch}$ or in both.

Around η=1 and below, the experimental ratio $E_{\rm T}/N_{\rm ch}$ is larger than that of both generators. The discrepancy in this zone seems to be due to a lack of $E_{\rm T}$ in the simulations, and the better quantitative agreement with VENUS 4.12 should be ascribed to the already noticed lack of charged pions. As there is no experimental result on identified particles in this zone, any more accurate analysis is prevented. We note, however, that the ratio of neutrons-to-protons is expected to approach that of the target in this zone, whereas it is lower in all simulations, although this fact alone cannot justify the discrepancy.

In the angular region covered by the HELIOS external spectrometer ($1 \leq \eta \leq 2$), the measured spectra and composition of identified particles, in particular the ratios p/K/π, lead to the observed value of about 0.7 GeV/charged particle[20]; similarly, around mid-rapidity ($2 \leq \eta \leq 3$), a region dominated by mesons, our result (0.6 to 0.7 GeV/charged particle) is consistent with other available data[1,21]. In this zone there is an overall agreement with VENUS 3.11 and with FRITIOF as well, though the shape of the distributions is very different. The disagreement with VENUS 4.12 can be ascribed both to the lack of charged pions and to the large contribution to $E_{\rm T}$ from the baryons (figure 7).

Around $\eta = 4$ (see figure 5), our data show a sizeable increase of the ratio $E_{\rm T}/N_{\rm ch}$, in contrast with the trend of all the simulations. Here, we cannot compare our result with that from other experiments, but note that the excess with respect to a reasonably monotonic decrease is 10% or more, one order of magnitude greater than the known systematic and statistical errors of our detectors[6-9]. It would be tempting to interpret this excess in terms of baryons not accounted for in the generators; however, in order to have an efficient mechanism, there should be on average around 10 more neutral baryons produced in this narrow window of rapidity. On the other hand, it can be seen that both FRITIOF and VENUS 4.12 produce in this zone a net number of baryons compatible with them being the remnants of the projectile, so that the excess should be in the form of neutral baryon-antibaryon pairs. This hypothesis could be supported by an enhancement of $E_{\rm T}$ in the experimental data noted in figure 4 around $\eta = 3.5$ (but mostly

in the sample of semicentral interactions !).

An alternative or complementary hypothesis could be that in the simulations there is a substantial lack of mesons (essentially π mesons) in the zone around $\eta = 2.5$, where the experimental values of E_T/N_{ch} show a valley. In other words, this would imply that rescattering is considerably more important than that accounted for by the generators. A hint in this direction could be not only the lack of E_T in the backward hemisphere, but also the lower experimental values of $< \eta >$ for all the samples as compared to the simulations, with a trend to produce even larger discrepancies for more central interactions and heavier targets (tables 2 and 3). Of course, the maximum effect is seen in the sample of S-W central interactions (figure 3), but the mechanism could be active in the other samples as well. In fact, we note from the generators that pions already show a low value of E_T/particle and since there are twice as many charged as neutral pions, there results an even lower value of E_T/charged particle when compared to that of kaons or baryons.

6 - Conclusions.

Taking advantage of the wide acceptance of both the emulsion detector and the HELIOS calorimeters, and by tagging central collisions, we have studied charged particle and transverse energy distributions in ^{32}S interactions at 200 GeV per nucleon on Ag and W targets.

Compared on the basis of normalized cross-sections, microscopic models like FRITIOF and VENUS ultimately fail to reproduce relevant experimental features, such as the absolute value of the global observables E_T and N_{ch}, their ratio, and the shape of their pseudorapidity distributions.

No threshold effect is apparent in the data as a function of centrality, whereas sizeable target effects were detected.

A detailed comparison between our data and those produced by the simulations strongly suggest an excess or a deficit of some production mechanism (such as baryon pairs or rescattering). Of course, an investigation based on the momentum distributions of identified particles, possibly over the whole range of pseudorapidity, would shed more light on the present data.

A comparison with collective models, although very appealing, is not yet possible due to major theoretical uncertainties still limiting the knowledge of pure/mixed phase equations of state and transport phenomena in relativistic ion collisions.

Acknowledgments

It is a pleasure to thank our colleagues of the HELIOS Collaboration who helped us through the various stages of the experiment. Helpful discussions with Dr. K. Werner about VENUS simulation were gratly appreciated.

References

(1) H. R. Schmidt and J. Schukraft, J. Phys G: Nucl. Part. Phys. **19** (1993)1705. See also the Proceedings of the last Quark Matter Conferences and references therein, e.g. Nucl. Phys. **A544** (1992), Nucl. Phys. **A566**(1994).

(2) B. Müller, "Physics and signatures of the Quark-Gluon Plasma", CERN preprint NUCL-TH-941005 (1994), submitted to Rep. Progr. Phys.; C. Gerschel, Nucl. Phys. **A583**(1995)643; S. Gavin et al., Z. Phys. **C61**(1994)351; A. Capella, "Strangeness enhancement in Heavy Ion Collisions", Orsay Preprint LPTHE 94-113 (1994).

(3) "Quark Gluon Plasma", Adv. series on Directions in High Energy Physics, Vol. **6** (World Scientific, 1990 - R.C. Hwa Editor).

(4) F. Karsch, Nucl. Phys. B (Proc. Suppl.) **34**(1994)63.

(5) E. Schnedermann and U. Heinz, Phys. Rev. **C50**(1994)1675.

(6) T.Åkesson et al., HELIOS-Emulsion Collaboration, Nucl. Phys. **B342**(1990)279.

(7) T. Åkesson et al., HELIOS Collaboration, Z. Phys. **C38**(1988)383; Phys. Lett. **B214**(1988)295.

(8) T.Åkesson et al., HELIOS Collaboration, Nucl. Phys. **B353** (1991)1.

(9) T. Åkesson et al., HELIOS Collaboration, Nucl. Phys. **B333** (1990)48.

(10) K. Werner, Z. Phys. **C42**(1989)85; K. Werner, Phys. Rep. **232**(1993)87.

(11) B. Andersson et al., Nucl. Phys. **A447**(1985)165c; B. Andersson et al., Nucl. Phys. **B281**(1987)289.

(12) K. Werner, "String Models for Ultrarelativistic Hadronic Interactions: Concepts, Limitations, and New Directions" Int. Workshop CORINNE-II, (Nantes, 1994), Heidelberg preprint HD-TVP-94-20 and CERN preprint NUCL-TH-9411033(1994).

(13) A. Capella et al., Phys. Rep. **236**(1994)225; J. Ranft et al., Phys. Lett.**B320**(1994)346; H.J. Moehring et al., Phys. Rev. **D47**(1993)4146.

(14) H. Sorge et al., Z. Phys. **C47**(1990)629; H. Sorge et al., Phys. Lett. **B289**(1992)6.

(15) M. Gonin et al., Phys. Rev. **C51**(1995)310.

(16) H.Sorge et al., Z. Phys. **C59**(1993)85.

(17) J.D. Bjorken, Phys. Rev. **D27**(1983)140; H. von Gersdoff, L. McLerran, M. Kataja and P.V. Ruuskanen, Phys. Rev. **D34**(1986)794; K.S. Lee, U. Heinz, E. Schnedermann, Z. Phys. **C48**(1990)525; D.H. Rischke, H. Stocker, W. Greiner, Phys. Rev. **D42**(1990)2283. J.-P. Blaizot and J.-Y. Ollitrault, Hydrodynamics of Quark-Gluon-Plasmas, ref (3), p. 393.

(18) L. Bravina et al., Phys. Rev. **C50**(1994)2161; S. Muroya et al., "Numerical Analyses of CERN 200 GeV/A Heavy-Ion Collisions Based on a Hydrodynamical Model with Phase Transition", CERN preprint NUCL-TH-9502002(1995).

(19) L. Van Hove, Phys. Lett. **118B**(1982)138; see also B. Müller in ref. (2).

(20) M. I. Adamovich et al., EMU01 Collaboration, Z. Phys. **C56**(1992)509.

(21) R. Albrecht et al., WA80 Collaboration, Z. Phys. **C55**(1992)539.

(22) R. Albrecht et al., WA80 Collaboration, Phys. Rev. **C44**(1991)2736; E. Andersen et al., NA36 Collaboration, Phys. Lett. **B294**(1992)127; T. Alber et al., NA35 Collaboration, Z. Phys. **C64**(1994)195.

(23) T. Åkesson et al., HELIOS Collaboration, Z. Phys. **C46**(1990)361; Z. Phys. **C46**(1990)369; Z. Phys. **C53**(1992)183.

Figure Captions :

Fig. 1 Differential $E_{\rm T}$ cross-section from ref. [8]: (a) Ag target, and (b) W target. Continuous and broken lines, respectively, refer to $E_{\rm T}$ distributions of minimum-bias events generated by VENUS (both 3.11 and 4.12) and FRITIOF (1.6).

Fig. 2 Correlation between $E_{\rm T}$ and $N_{\rm ch}$. Entries from individual events on emulsion (open circles) and W targets (dots). Crosses represent VENUS and FRITIOF results; no target dependence is observed. For each cross, the horizontal arm indicates the $E_{\rm T}$ bin and the vertical arm the $N_{\rm ch}$ standard deviation.

Fig. 3 Pseudorapidity density distributions $\frac{1}{N_{\rm ev}} \frac{dN_{\rm ch}}{d\eta}$ for semicentral and central event classes, separately shown for each target. Dots refer to experimental data, lines to VENUS and FRITIOF, respectively.

Fig. 4 Pseudorapidity $E_{\rm T}$-distributions $\frac{1}{N_{\rm ev}} \frac{dE_{\rm T}}{d\eta}$, for the same classes as in Fig. 3. Graphic symbols as in Fig. 3.

Fig. 5 Pseudorapidity distributions of the ratio $\frac{<E_{\rm T}>}{<N_{\rm ch}>}$, for the same classes as in Fig. 3 and 4. Graphic symbols as in Fig. 3 and 4. The vertical bars indicate the error on the mean ratio, as estimated by its standard deviation in each η bin.

Fig. 6 Pseudorapidity density distributions $\frac{1}{N_{\rm ev}} \frac{dN}{d\eta}$ for separate charged particles obtained from the models in central S-W interactions.

Fig. 7 Pseudorapidity $E_{\rm T}$-distributions $\frac{1}{N_{\rm ev}} \frac{dE_{\rm T}}{d\eta}$, for separate particles obtained from the models in central S-W interactions.

	N. of events	E_T (GeV)			$< N_{ch} >$	rms	$\frac{<E_T>}{<N_{ch}>}$ (GeV)
		min	max	aver.			
S-Ag Semicentral							
Data	119	195	263	222	319	42	0.70
VENUS 3.11	530	184	258	217	339	39	0.64
VENUS 4.12	564	190	254	214	284	30	0.75
FRITIOF	581	180	242	206	332	32	0.62
S-Ag Central							
Data	58	263	-	275	389	39	0.71
VENUS 3.11	259	258	-	275	435	35	0.63
VENUS 4.12	131	254	-	272	357	24	0.76
FRITIOF	191	242	-	254	404	26	0.63
S-W Semicentral							
Data	111	258	326	284	422	51	0.67
VENUS 3.11	461	262	325	288	462	40	0.62
VENUS 4.12	451	244	316	283	371	28	0.76
FRITIOF	494	244	290	261	422	29	0.62
S-W Central							
Data	30	326	-	334	502	47	0.66
VENUS 3.11	163	325	-	334	537	28	0.62
VENUS 4.12	126	316	-	333	434	25	0.77
FRITIOF	170	290	-	298	477	28	0.62

Table 1 : Global features of measured data and simulated events, both selected according to E_T and to the criteria discussed in the text; secondaries in the range $0.6 \leq \eta \leq 5.5$.

S - Ag

	Semicentral			Central		
	$(\frac{dN_{ch}}{d\eta})_{max}$	$<\eta>$	σ	$(\frac{dN_{ch}}{d\eta})_{max}$	$<\eta>$	σ
Data	91.7	2.98	1.59	118.3	2.82	1.45
VENUS 3.11	102.1	3.13	1.44	134.0	3.08	1.40
VENUS 4.12	95.6	3.07	1.55	107.0	2.95	1.46
FRITIOF	95.6	3.06	1.55	118.4	2.99	1.51

S - W

	Semicentral			Central		
	$(\frac{dN_{ch}}{d\eta})_{max}$	$<\eta>$	σ	$(\frac{dN_{ch}}{d\eta})_{max}$	$<\eta>$	σ
Data	122.7	2.70	1.61	153.0	2.58	1.52
VENUS 3.11	139.8	3.02	1.43	166.7	2.94	1.39
VENUS 4.12	108.3	2.86	1.52	130.8	2.81	1.46
FRITIOF	123.9	2.92	1.52	141.0	2.84	1.49

Table 2 : Maximum charged multiplicity densities, mean and r.m.s. values of η from a Gaussian fit to the experimental and simulated data.

S - Ag

	Semicentral			**Central**		
	$(\frac{dE_T}{d\eta})_{\max}$ (GeV)	$<\eta>$	σ	$(\frac{dE_T}{d\eta})_{\max}$ (GeV)	$<\eta>$	σ
Data	65.6	2.91	1.57	81.8	2.70	1.55
VENUS 3.11	67.4	3.00	1.38	87.5	2.94	1.33
VENUS 4.12	66.0	2.93	1.40	87.1	2.87	1.32
FRITIOF	61.6	3.02	1.46	77.8	2.94	1.41

S - W

	Semicentral			**Central**		
	$(\frac{dE_T}{d\eta})_{\max}$ (GeV)	$<\eta>$	σ	$(\frac{dE_T}{d\eta})_{\max}$ (GeV)	$<\eta>$	σ
Data	81.5	2.56	1.73	99.1	2.39	1.63
VENUS 3.11	89.9	2.86	1.36	107.2	2.79	1.32
VENUS 4.12	88.3	2.77	1.38	108.4	2.72	1.30
FRITIOF	79.2	2.89	1.43	92.2	2.82	1.39

Table 3 : Maximum transverse energy densities, mean and r.m.s. values of η from a Gaussian fit to the experimental and simulated data.

S - Ag

		Semicentral			Central			N max
		F.	V. 3.11	V. 4.12	F.	V. 3.11	V. 4.12	
Net n. of baryons	charged	28	36	34	36	46	41	47
	neutral	36	36	40	45	45	48	57
Total		64	72	70	81	91	89	104
Antibaryons		10	24	9	12	36	10	-

S - W

		Semicentral			Central			N max
		F.	V. 3.11	V. 4.12	F.	V. 3.11	V. 4.12	
Net n. of baryons	charged	38	54	48	45	62	56	51
	neutral	50	54	59	58	65	67	67
Total		88	108	107	103	127	123	118
Antibaryons		13	40	11	14	51	13	-

Table 4 : Net number of baryons and number of antibaryons in semicentral and central S-Ag and S-W interactions ($0.6 \leq \eta \leq 5.5$) according to various models (F. = FRITIOF; V.= VENUS).

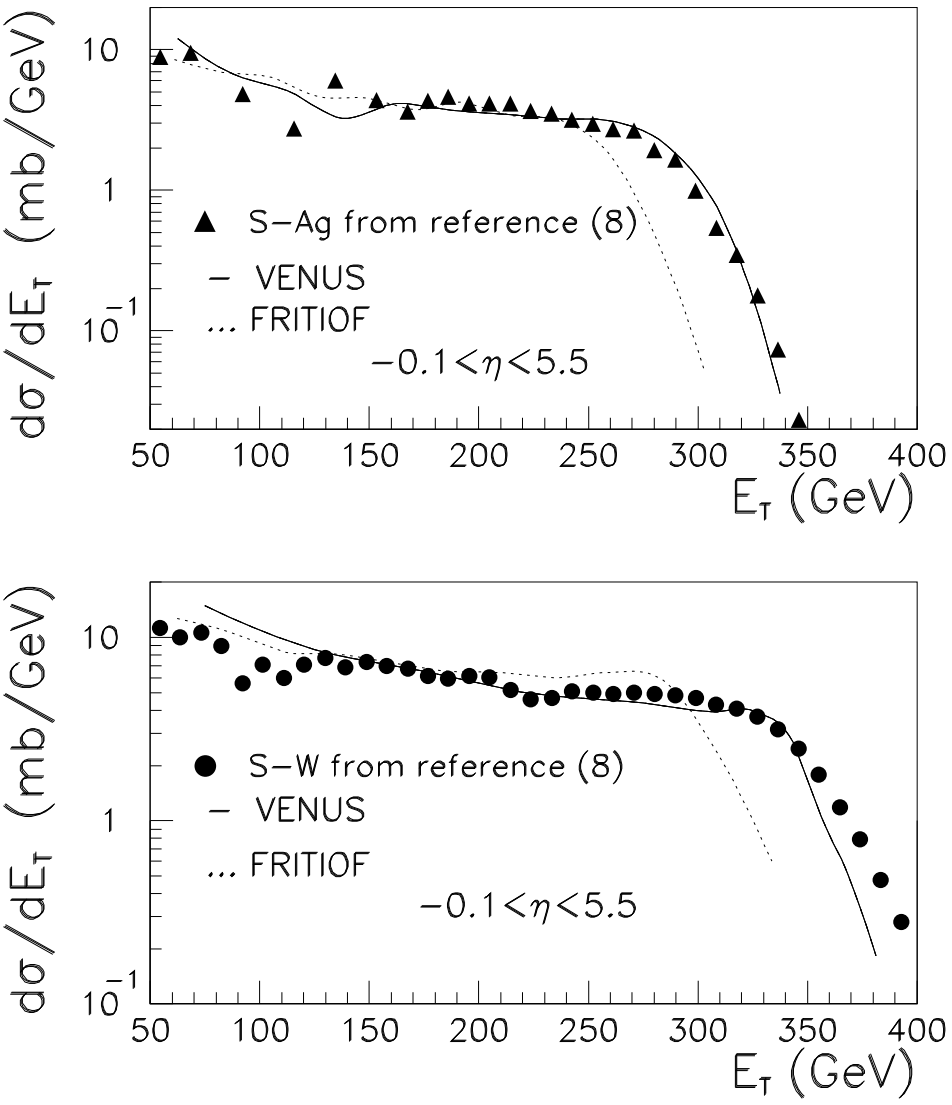
dσ/dE_T (mb/GeV)
10
1
10^-1
S–Ag from reference (8)
– VENUS
... FRITIOF
–0.1<η<5.5
50
100
150
200
250
300
350
400
E_T (GeV)
dσ/dE_T (mb/GeV)
10
1
10^-1
S–W from reference (8)
– VENUS
... FRITIOF
–0.1<η<5.5
50
100
150
200
250
300
350
400
E_T (GeV)

Figure 1:

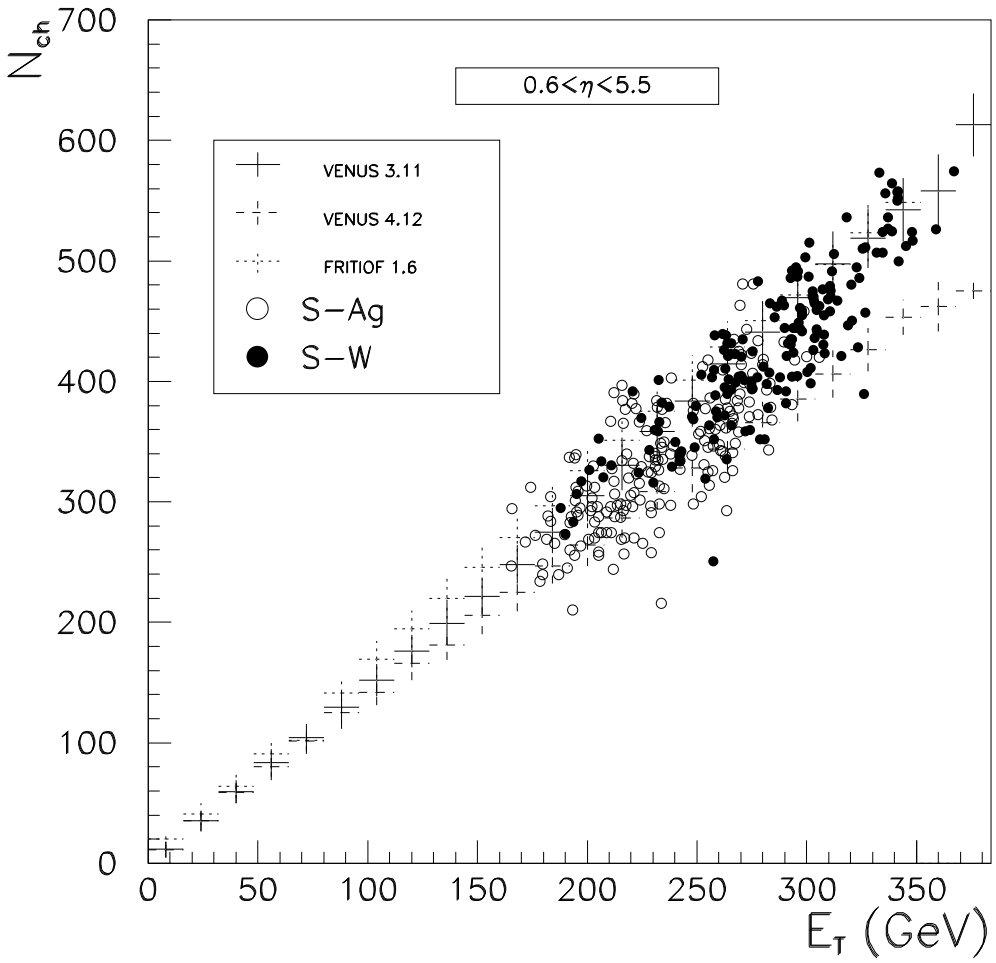
N_{ch}
700
600
500
400
300
200
100
0
0.6<η<5.5
VENUS 3.11
VENUS 4.12
FRITIOF 1.6
S−Ag
S−W
0
50
100
150
200
250
300
350
E_T (GeV)

Figure 2:

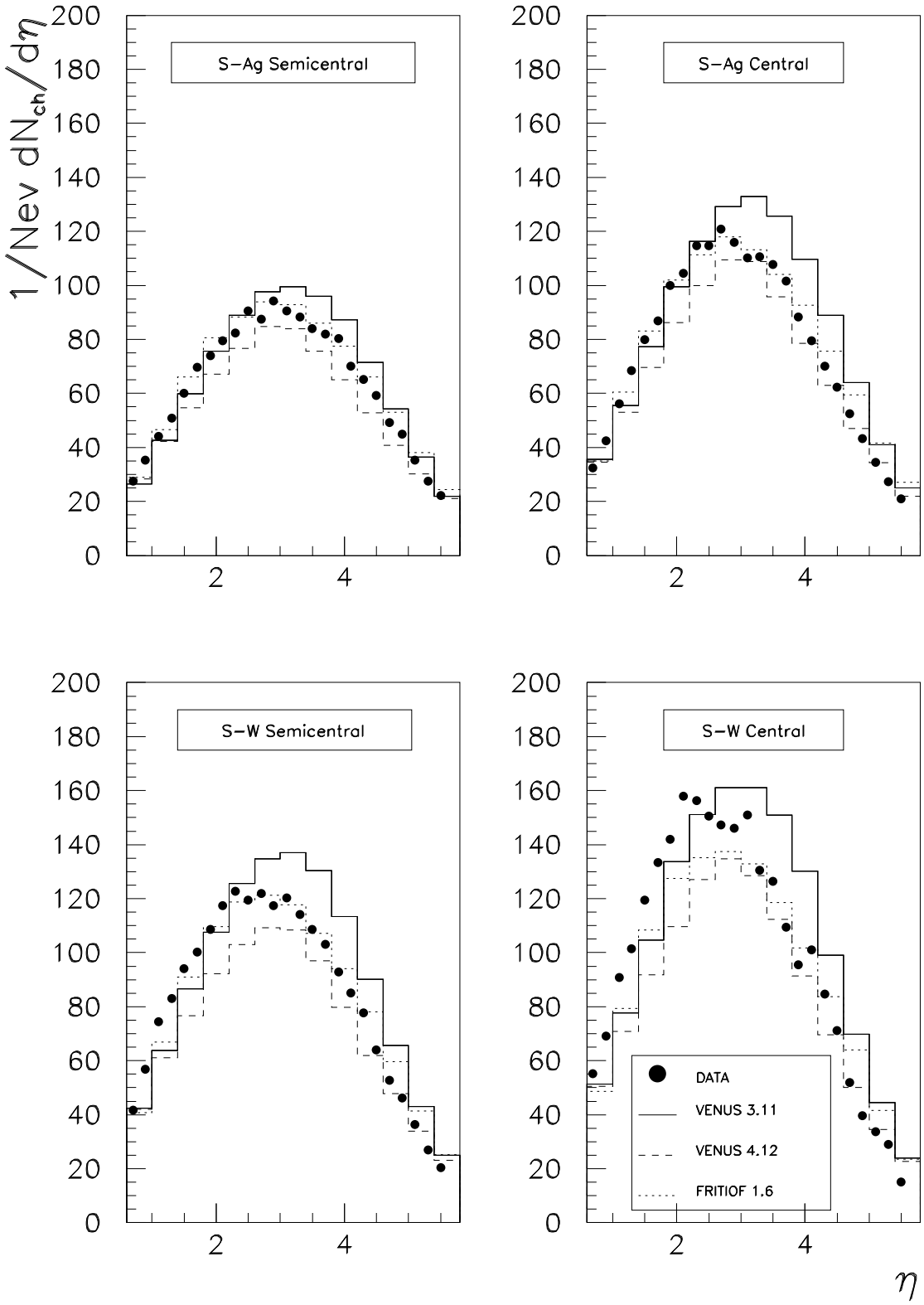
1/Nev dN_ch/dη
S−Ag Semicentral
S−Ag Central
S−W Semicentral
S−W Central
DATA
VENUS 3.11
VENUS 4.12
FRITIOF 1.6
η

Figure 3:

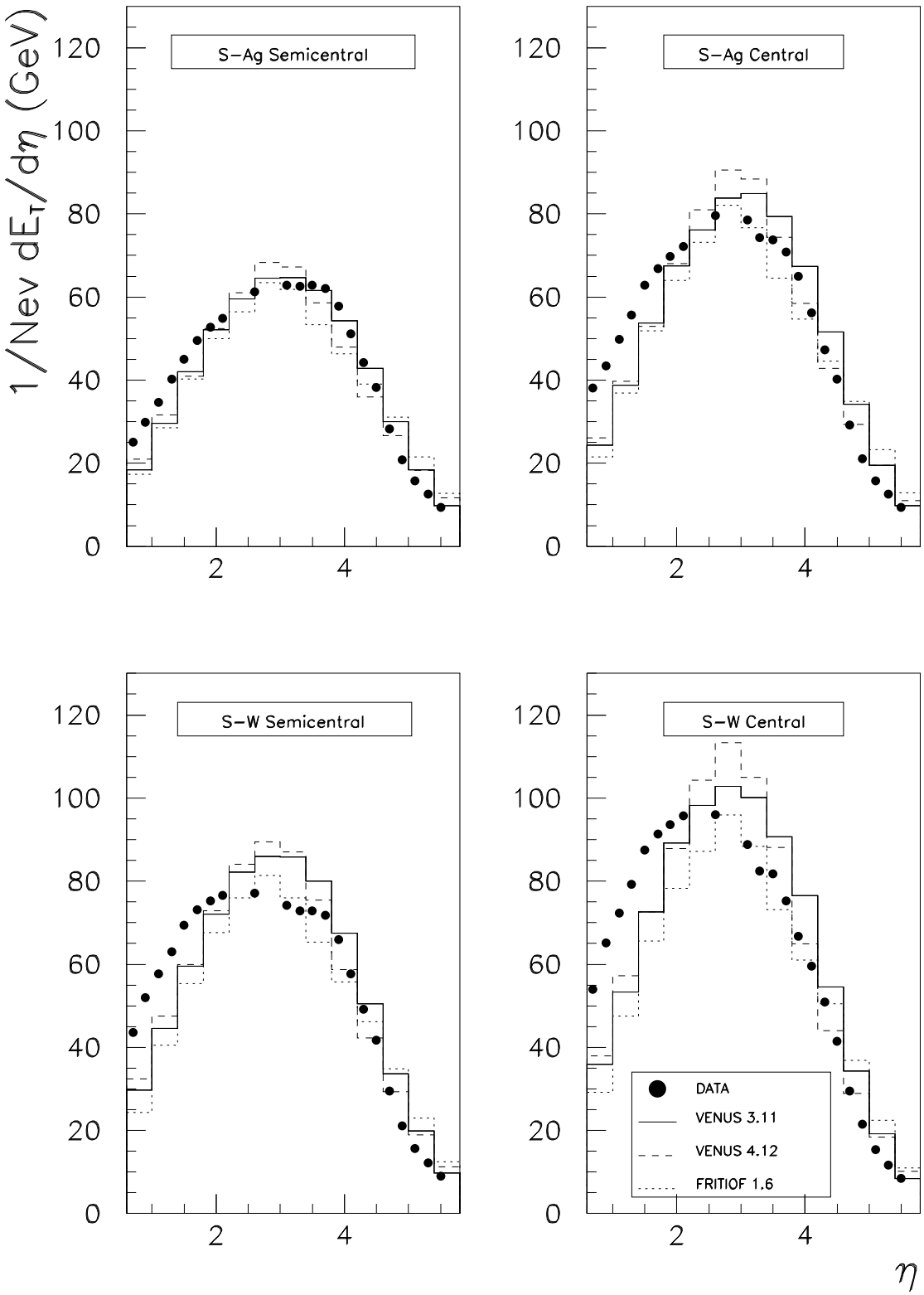
1/Nev dE_T/dη (GeV)
S−Ag Semicentral
S−Ag Central
S−W Semicentral
S−W Central
DATA
VENUS 3.11
VENUS 4.12
FRITIOF 1.6
η

Figure 4:

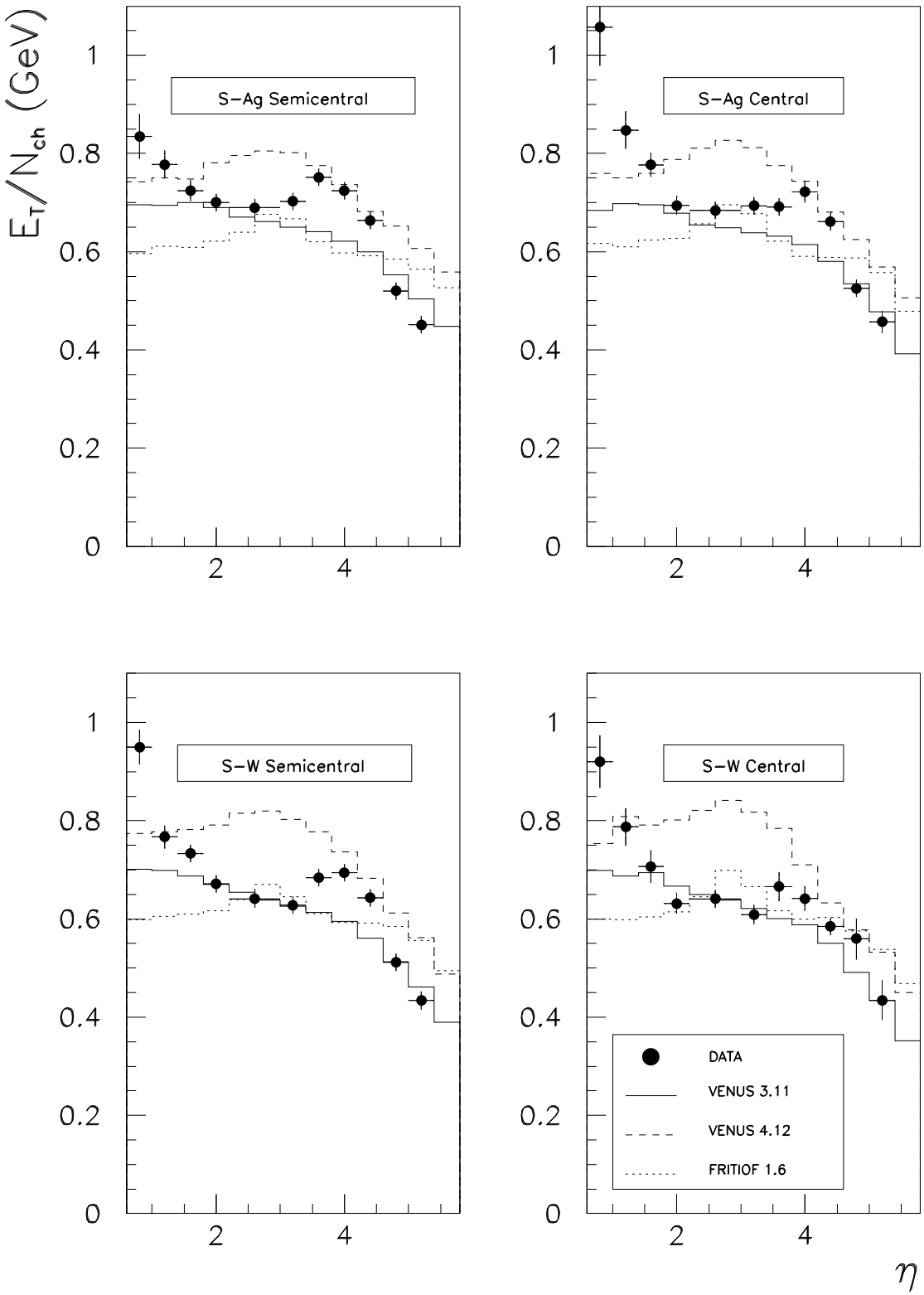
E_T/N_{ch} (GeV)
S−Ag Semicentral
S−Ag Central
S−W Semicentral
S−W Central
DATA
VENUS 3.11
VENUS 4.12
FRITIOF 1.6
η

Figure 5:

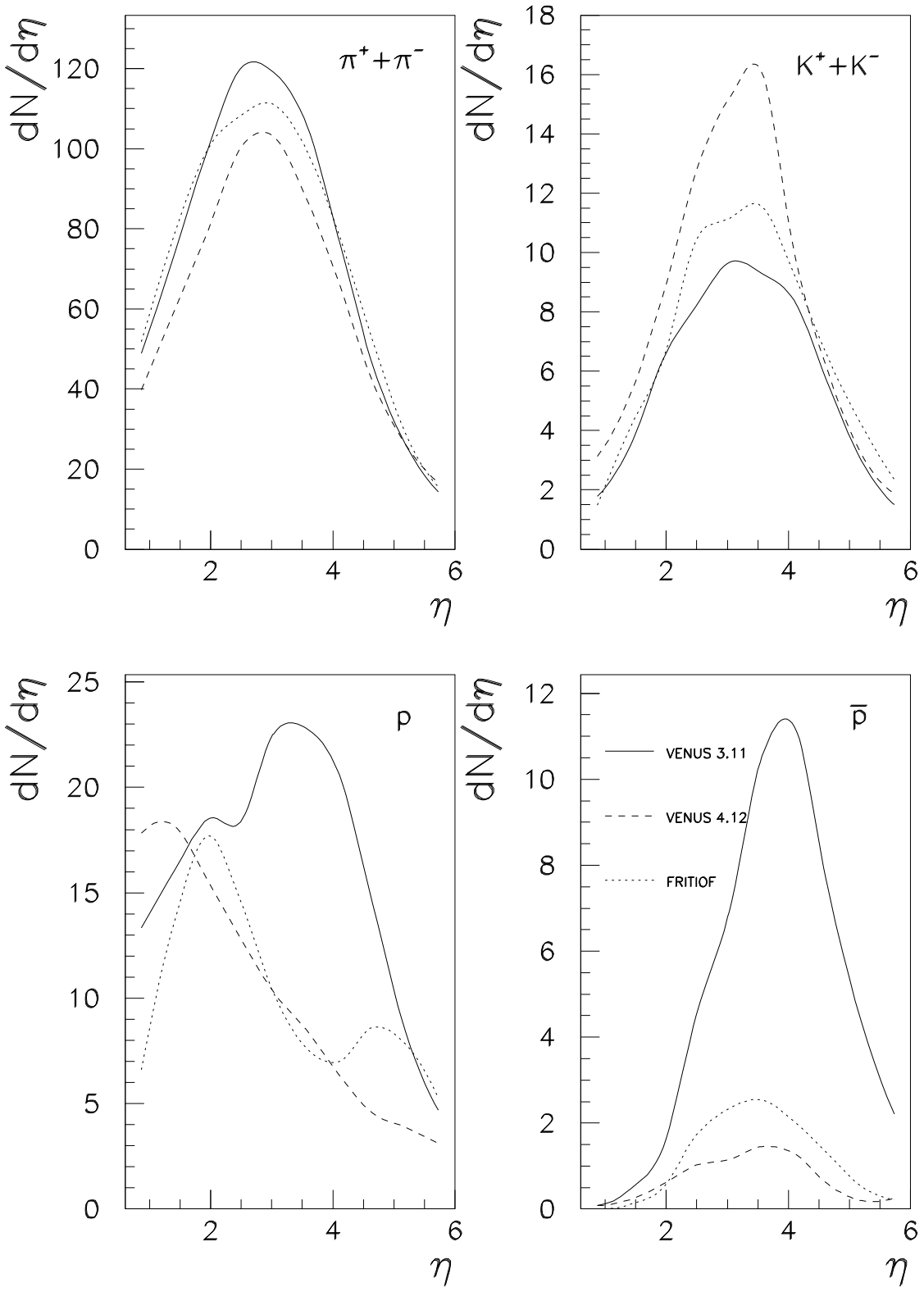

Figure 6:

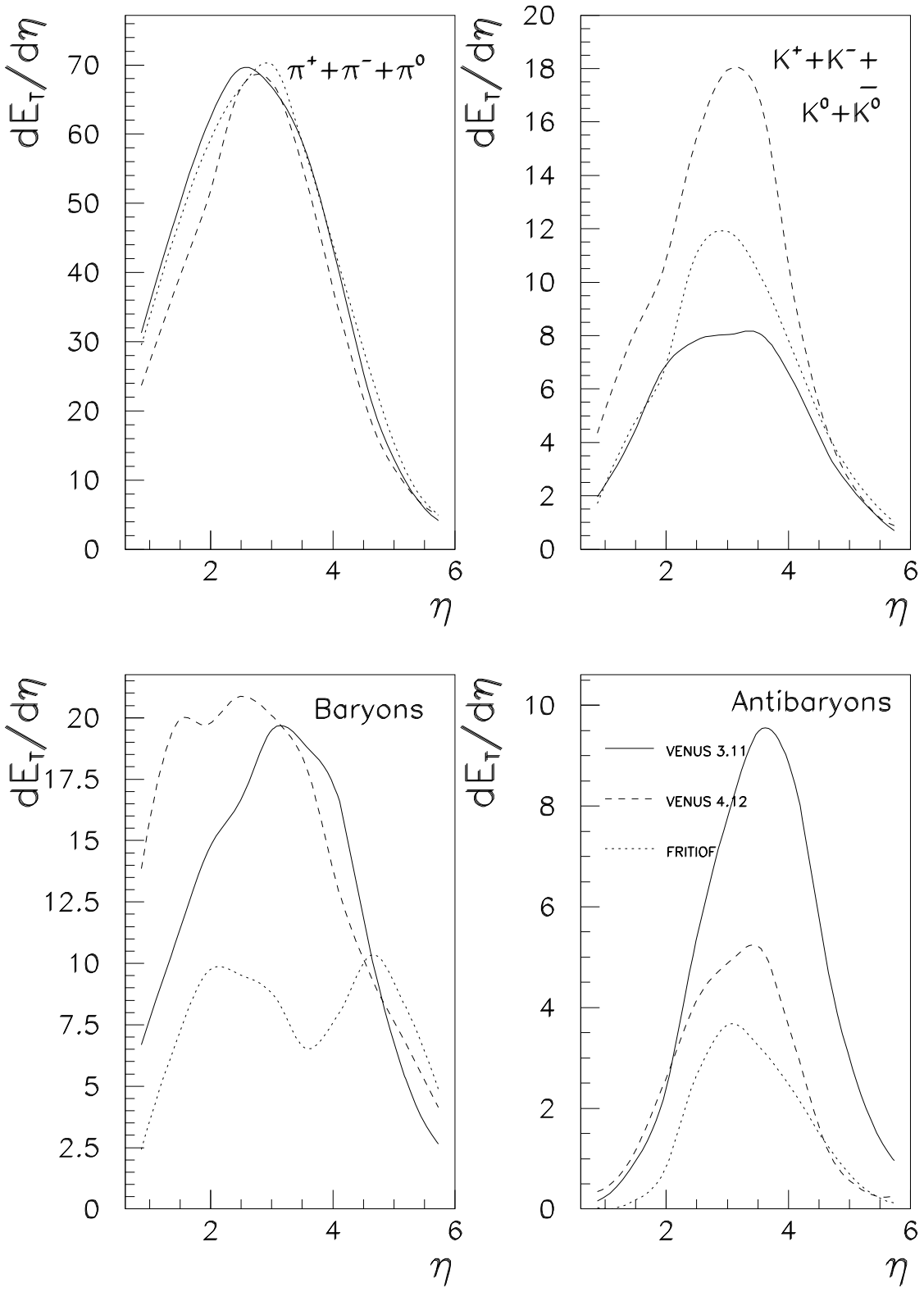
dE_T/dη
π⁺+π⁻+π⁰
K⁺+K⁻+
K⁰+K̄⁰
Baryons
Antibaryons
VENUS 3.11
VENUS 4.12
FRITIOF
η

Figure 7: